Computer Science Department, University of Auckland
CITR at Tamaki Campus (http://www.tcs.auckland.ac.nz/)

CS-TR-150 / CITR-TR-8 July 1997

Sound Analysis of 3D Objects Based on Digitized Data

Reinhard Klette*

Abstract

The paper reviews selected results in the field of geometrical measurements and reconstructions of 3D objects based on gridding techniques. Two soundness properties of approaches are discussed with respect to the selected grid resolution: *convergence* and *convergence towards the proper value*. It is shown that sound approaches exist for problems as (1) volume and surface area measurement for Jordan bodies, (2) approximations of planes based on sampled data, (3) surface reconstructions based on gradient information, and (4) surface recovery by solving a (special) linear differential equation system. The paper concludes with a brief discussion of arising digital or computational geometry problems relevant to the discussed subjects.

* The University of Auckland, Tamaki Campus, Computing and Information Technology Research, Computer Vision Unit, Auckland, New Zealand

Sound Analysis of 3D Objects Based on Digitized Data

Reinhard Klette
Computer Science Department, Tamaki Campus
University of Auckland
New Zealand

Abstract: The paper reviews selected results in the field of geometrical measurements and reconstructions of 3D objects based on gridding techniques. Two soundness properties of approaches are discussed with respect to the selected grid resolution: *convergence* and *convergence towards the proper value*. It is shown that sound approaches exist for problems as (1) volume and surface area measurement for Jordan bodies, (2) approximations of planes based on sampled data, (3) surface reconstructions based on gradient information, and (4) surface recovery by solving a (special) linear differential equation system. The paper concludes with a brief discussion of arising digital or computational geometry problems relevant to the discussed subjects.

1 Introduction

This paper deals with objects (bodies, surfaces, faces, planes etc.) in three-dimensional (3D) space that are represented by digital images or discrete data arrays. Image analysis of the three-dimensional objects is based on the given digitized data. The input information may be a *voxel data set*, where *voxel* stands for *volume element* which is the sample value at a grid point, or it may be one or several digitized projections of real-world scenes. Example application areas are biomedical 3D image analysis, or industrial surface inspection, respectively. The analysis task is directed towards reconstructing or analyzing an unknown 3D object which may be considered to form a compact set in the 3D Euclidean space $\mathbf{R}^3$ bounded by a *Jordan surface*, or just an unknown *Jordan face* in 3D. This paper is not a general review. It is based on some subjective selections of relevant results (without citing proofs) in this area of geometrical measurements and reconstructions based on gridding techniques.

1.1 Soundness Properties

The length of a diagonal of a square with side length a can not be measured via the length of a piecewise constant function because the total length of the piecewise constant function is always $2a$ independent of the number or the size of the steps, and does not converge towards $a\sqrt{2}$ if the step-size goes to zero. This is a popular example of the following problem: assume that a real-world object is given and we have only some sampled or digitized data about this object. What is the appropriate method to calculate a specific feature of this object, or to represent it?

The measurement of areas in 2D, or of volumes in 3D is normally much more robust or straightforward than measurement of perimeters in 2D, or of surface areas in 3D. For the "diagonal of a square" example above the size of the area below the "diagonal" piecewise constant function will converge to the size of the triangle defined by two sides of the square and the diagonal if the step size goes to zero.

Digital geometry approaches, computational geometry algorithms and further calculations (numerics, statistics etc.) may be used to represent and analyze the given discrete data. The approach should be *sound with respect to the general measurement or representation problem*. We consider the following two soundness properties in this paper:

CONVERGENCE: Image acquisition at higher image resolutions should lead to convergence for the values of measured features, such as the geometric shape of reconstructed planes, straight lines, surfaces etc.

PROPER VALUE: Convergence should be towards the "true" value, the "true" data etc.

The first soundness property requires a convergence proof. The diagonal in the example above converges towards $2a$. The second soundness property requires a fundamental problem analysis: what is the "true data", the so-called *ground truth*? Certainly the "true" data is unknown in applications of image analysis. Synthetic input data may be a solution. However these are always just case studies for a specific type of hypothetical input data. The complete solution is the mathematical modeling of the measurement or representation problem where the ground truth is defined in general mathematical terms. It is easy to model a plane, a polygonal face or a straight line. The diagonal in the example above has

length $a\sqrt{2}$. A general surface model needs more explanation and is discussed below.

An evaluation approach based on a general mathematical model of the ground truth does not require experiments with real or synthetic input data (besides that, such experiments may be useful to illustrate or to validate), and is restricted to a the class of precisely definable problems.

1.2 Jordan Faces

C. Jordan is already famous in the image analysis literature for his curve theorem often cited for separations in 2D. A generalization of this Jordan curve theorem is also valid for specific sets of points in 3D allowing a general definition of a 3D objects which we call *Jordan bodies*. Such a Jordan body is given as a voxel data set and must be analyzed based on this discrete information which is characterized by a given resolution, and also by a geometric model (as polyhedron, or "smooth surface object") of the unknown Jordan body.

What is the "true" surface area? This question is easy to answer for planar, polygonal object faces. But what about curved objects?

Fortunately integration and differentiation techniques for modeling surfaces in 3D were already studied in mathematics since the 19th century, see No. 109 in [19], and provide the proper approaches for modeling and measuring of object surfaces. At first we assume a segmentation of 3D object surfaces into several faces.

Definition 1 (Jordan Face): A *Jordan face* $\mathbf{F}$ in 3D Euclidean space $\mathbf{R}^3$ is a set of points $\mathbf{F} \subseteq \mathbf{R}^3$ which may be parameterized as $\mathbf{F} = \mathbf{F}_\mathbf{B}(\varphi, \psi, \chi)$ by a simply connected compact set $\mathbf{B} \subseteq \mathbf{R}^2$ and three functions φ, ψ, and χ differentiable for all positions (u,v) in $\mathbf{B}$, where

$$\mathbf{F}_\mathbf{B}(\varphi, \psi, \chi) = \{(x,y,z) : x = \varphi(u,v) \wedge y = \psi(u,v) \wedge z = \chi(u,v) \wedge (u,v) \in \mathbf{B}\},$$

and for which it is assumed that each point in $\mathbf{F}_\mathbf{B}(\varphi, \psi, \chi)$ is defined by exactly one point $(u,v) \in \mathbf{B}$, and that the rank of the matrix of the first derivatives

$$\begin{pmatrix} \varphi_u & \psi_u & \chi_u \\ \varphi_v & \psi_v & \chi_v \end{pmatrix}$$

is equal to two for all positions (u,v) in $\mathbf{B}$.

From this definition it follows that at each position $\mathbf{b} = (u,v)$ at least one of the three subdeterminants

$$A=\begin{vmatrix}\psi_u & \chi_u\\ \psi_v & \chi_v\end{vmatrix},\ B=\begin{vmatrix}\chi_u & \varphi_u\\ \chi_v & \varphi_v\end{vmatrix},\ \text{and}\ C=\begin{vmatrix}\varphi_u & \psi_u\\ \varphi_v & \psi_v\end{vmatrix}$$

is not equal to zero. These subdeterminants may be used to define the area $J_{area}(\mathbf{F})$ of face $\mathbf{F}$ as follows

$$J_{area}(\mathbf{F})=\int_{\mathbf{B}}\sqrt{A^2+B^2+C^2}\,d\mathbf{b}$$

assuming that $\mathbf{F}$ is measurable (see Definition 3 below).

For example assume any simply connected, planar, compact face $\mathbf{F}$. Then $\mathbf{B}$ may be chosen parallel to the $\mathbf{F}$ plane, with $\varphi(u,v)=\text{const}$, $\psi(u,v)=u$, and $\chi(u,v)=v$. The rank of the corresponding matrix

$$\begin{pmatrix}0 & 1 & 0\\ 0 & 0 & 1\end{pmatrix}$$

is two and the equation

$$J_{area}(\mathbf{F})=\int_{\mathbf{B}}d\mathbf{b}=J_{area}(\mathbf{B})$$

reduces the 3D measurement problem to a 2D measurement problem. It follows that any simply connected, planar, compact set $\mathbf{F}$ is a Jordan face according to the definition above, and it is measurable if its 2D projection is measurable.

The measurability definition [19] of Jordan faces $\mathbf{F}=\mathbf{F}_{\mathbf{B}}(\varphi,\psi,\chi)$ is based on a triangulation of a bounded superset $\mathbf{B}_1$ of $\mathbf{B}$ satisfying $\mathbf{B}\subseteq I(\mathbf{B}_1)$, where $I(\mathbf{B}_1)$ denotes the *interior* of the set $\mathbf{B}_1$, and the first order derivatives of the functions φ, ψ, χ exist and they are continuous in $I(\mathbf{B}_1)$. Formally this means that $\varphi,\ \psi,\ \chi\in C^{(1)}\left(I(\mathbf{B}_1)\right)$. In No. 108 of [19] it is shown that the angles α of such triangulations (of the base sets of the resulting polyhedral faces) have to satisfy the constraint $\alpha<2\pi/3$ (independently shown by *O. Hölder* in 1882, *G. Peano* in 1890, and *H. A. Schwarz* in 1890) to avoid inaccurate surface value calculations for curved surfaces. This might also be cited as a remarkable result for triangulations in modern computer graphics.

Definition 2 (Triangular Subdivision): Let $\mathbf{B}_1\subseteq\mathbf{R}^2$ be a simply connected compact set with $\mathbf{B}\subseteq I(\mathbf{B}_1)$ and assume an angle ω with $0<\omega<\pi/3$. Then any network Z of triangles completely covering $\mathbf{B}_1$ and satisfying the following two properties,

(i) all angles of triangles in Z are less or equal to $\pi - \omega$, and

(ii) for all triangles in Z having at least one point in common with set $\mathbf{B}$ it holds that all three corner points are in set $\mathbf{B}_1$,

is called a *triangular subdivision Z of $\mathbf{B}_1$ with respect to $\mathbf{B}$*.

Definition 3 (Measurable Jordan Face): Let $\mathbf{F} = \mathbf{F}_\mathbf{B}(\varphi, \psi, \chi)$ be a Jordan face. The face $\mathbf{F}$ is *measurable* if there exists a simply connected compact set $\mathbf{B}_1 \subseteq \mathbf{R}^2$ such that $\mathbf{B} \subseteq I(\mathbf{B}_1)$, the functions φ, ψ, χ are in $C^{(1)}(I(\mathbf{B}_1))$, and there exists a sequence Z_1, Z_2, Z_3, ... of triangular subdivisions of $\mathbf{B}_1$ with respect to $\mathbf{B}$ such that

$$a_t \to 0$$

where a_t denotes the maximum length of any side of any triangle in the subdivision Z_t.

Each triangular subdivision Z *of* $\mathbf{B}_1$ with respect to $\mathbf{B}$ defines a polyhedral approximation $\mathbf{F}(Z)$ of the given Jordan face $\mathbf{F} = \mathbf{F}_\mathbf{B}(\varphi, \psi, \chi)$.

Jordan Face Area Theorem: *A measurable Jordan face allows the formation of an infinite sequence of polyhedral approximations $\mathbf{F}(Z_1)$, $\mathbf{F}(Z_2)$, $\mathbf{F}(Z_3)$, ... having well-defined surface areas $J_{area}(\mathbf{F}(Z_1))$, $J_{area}(\mathbf{F}(Z_2))$, $J_{area}(\mathbf{F}(Z_3))$, ... which converge to*

$$J_{area}(\mathbf{F}) = \int_{\mathbf{B}} \sqrt{A^2 + B^2 + C^2}\, d\mathbf{b}$$

independent of the chosen parametrization $\mathbf{B}$, φ, ψ, and χ, and independent of the chosen sequence of triangular subdivisions.

This theorem is a historic result about Jordan faces, and a complete proof may be found in [19]. It points out that a proof about the measurability of a given Jordan face (and its value of the surface area) may be based on just one selected parametrization of this face, and on just one selected triangular subdivision satisfying the angle constraint as specified in Definition 2.

1.3 Jordan Surfaces

A single Jordan face is not a complete surface of a 3D body. Because of the assumed property that each point in $\mathbf{F}_\mathbf{B}(\varphi, \psi, \chi)$ is defined by exactly one point

$(u,v) \in \mathbf{B}$ it follows that at least two faces are necessary to obtain a closed surface of a 3D object. Furthermore, the assumed $C^{(1)}$ property of functions φ, ψ, χ allows no discontinuities within a single Jordan face, as it appears at edges of polyhedral objects. A *polyhedron* is a simply connected compact set where the boundary consists of a finite number of simply connected planar compact sets. A single Jordan face can not in general be "the edge" of a polyhedron.

Definition 4 (Jordan Body, Jordan Surface, Surface Area): A *Jordan body* is a simply connected compact set $\Theta \subset \mathbf{R}^3$ the boundary of which consists of a finite number of measurable Jordan faces $\mathbf{F}_1$, $\mathbf{F}_2$, ..., $\mathbf{F}_n$. A *Jordan surface* $\mathbf{S} = \mathbf{S}(\Theta)$ is the boundary $\partial\Theta$ of a Jordan body Θ, i.e. $\mathbf{S} = \mathbf{F}_1 \cup \mathbf{F}_2 \cup ... \cup \mathbf{F}_n$. Assuming that the 2D interiors of the sets $\mathbf{F}_t$ are pairwise disjoint the *surface area* of $\mathbf{S}$ is defined as $J_{area}(\mathbf{S}) = J_{area}(\mathbf{F}_1) + J_{area}(\mathbf{F}_2) + ... + J_{area}(\mathbf{F}_n)$.

The open set $I(\Theta) = \Theta - \partial\Theta$ is the *interior* of this Jordan surface $\mathbf{S}$. A Jordan body is always homeomorphic to a unit ball, and a Jordan surface is always homeomorphic to the unit sphere, i.e. the surface of the unit ball. Each polyhedron is a Jordan body and many curved objects may be classified to be Jordan bodies. A *smooth Jordan surface* is a Jordan surface which possesses a tangent plane in each of its points, which is not necessarily the case for a union of measurable Jordan faces. The following Theorem holds for smooth, and also for non-smooth Jordan surfaces.

Jordan Surface Theorem: *Any Jordan surface* $\mathbf{S}$ *subdivides the* $\mathbf{R}^3$ *into three disjoint set, its interior* $\mathbf{I}$*, the set* $\mathbf{S}$ *itself, and a set* $\mathbf{E} = \mathbf{R}^3 - (\mathbf{S} \cup \mathbf{I})$ *where* $\mathbf{I}$ *and* $\mathbf{E}$ *are open sets with* $\partial\mathbf{I} = \partial\mathbf{E} = \mathbf{S}$.

The open set $\mathbf{E} = E(\mathbf{S})$ is the *exterior* of this Jordan surface $\mathbf{S}$. "Going from $\mathbf{I}$ to $\mathbf{E}$" means that we have "to leave $\mathbf{I}$" by passing through its boundary $\partial\mathbf{I} = \mathbf{S}$, i.e. any curve starting in $\mathbf{I}$ and ending in $\mathbf{E}$ intersects the given surface $\mathbf{S}$ at least once. A Jordan surface specifies a separation in 3D as a Jordan curve does in 2D.

Many imaging processes such as Computer Tomography (CT), Magnetic Resonance Imaging (MRI) or Confocal Microscopy (CSLM), provide a series of aligned planar scans which together comprise a special voxel data set, a *voxel data cube*. Some microscope image analysis processes are based on digitized slices of objects where at first the obtained images have to be aligned. However, assuming correct alignment also in these cases such a voxel data cube is given describing a certain 3D object. The object Θ of interest, represented in this data

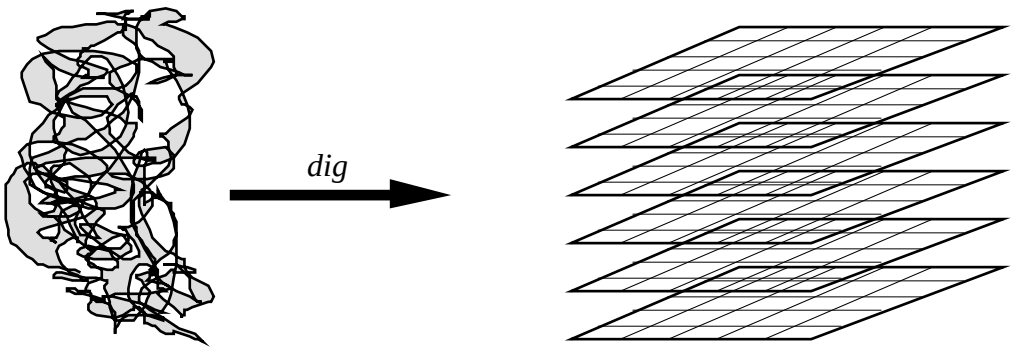

Figure 1: An unknown object Θ, the ground truth, is represented after image acquisition as $dig(\Theta)$, and this information is "hidden" within a voxel data cube f of labeled grid points.

cube, is normally given as a fuzzy set and not defined by a Jordan surface. However we assume from now on that the 3D object Θ is a Jordan body. The treatment of 3D objects with fuzzy surfaces is not covered in this paper. This requires a non-trivial extension of the Jordan body model.

So far the *true surface area* of a 3D object is specified, and further *true features* (as volumes $J_{volume}(\Theta)$, centroids, moments, potentials etc. of Jordan bodies Θ) may be uniquely defined following classical mathematical texts as [19].

Image acquisition may be modeled at a certain level of abstraction as a mapping of a given Jordan body, which is surrounded by further Jordan bodies, into a digital space. Techniques generating a voxel data cube (see Fig. 1) are mapping the whole Jordan body and its surrounding set into a certain grid. Techniques based on projective mappings produce some projective images of the given Jordan body within specified image grids. The next section deals with the digitization process related to the first approach sketched in Fig. 1.

2 Object Digitization

Grids (not only orthogonal ones) were introduced by *C. Jordan* and *G. Peano* around 1890 for defining measurable sets (now known as the *Jordan*, or the *Jordan-Peano area* of a point set). The formation of *digital geometry* as a fundamental subject in image analysis by *A. Rosenfeld* around 1965 was an important step for establishing a scientific approach in image analysis in contrast to an

engineering or application oriented approach. The mapping of "real objects" into grid point sets was always an inherent problem in digital geometry, and several models are in use as an abstraction of image acquisition processes.

2.1 Orthogonal Grids at Different Resolutions

We assume labeled points **p** in the 3D orthogonal grid, with integer coordinates (i,j,k) at grid point positions, to be the raw representation of the digitized object data, where $1 \le i,j,k \le N$. In the case of *binary labels* we assume either $f(i,j,k)=0$ or $f(i,j,k)=1$, and 0 means that the grid point is "not in the object', and 1 means that the grid point is "inside of the object". In the case of *fuzzy labels* $f(i,j,k)=u$ in the interval $[0,1]$ it is normally intended that label u means that a grid point is an object point "with fuzzy weight u". For example assume grey value images and a threshold T for separating object from background image values. Then u may be defined by a certain normalized distance between the current image value and the threshold value T.

A voxel data cube f may be described as being an $N \times N \times N$ set of labeled grid points. We consider only the binary 3D cubic grid model in this paper which is also considered in [16]. Orthogonal grids subdivide the space $\mathbf{R}^3$ with different resolutions, say 2^{-r} with $r = 0,1,2,...$, where each *grid point* (i,j,k) having integer coordinates represents a *cell*

$$\mathbf{C}_r(i,j,k) = \left\{(x,y,z) \in \mathbf{R}^3 : x \in [i]_r \wedge y \in [j]_r \wedge z \in [k]_r\right\}$$

in $\mathbf{R}^3$, with $[m]_r = \left\{x : \left(m-\tfrac{1}{2}\right)\cdot 2^{-r} \le x \le \left(m+\tfrac{1}{2}\right)\cdot 2^{-r}\right\}$ for an integer m. Each cell is a Jordan body, it has a volume of

$$J_{volume}\left(\mathbf{C}_r(i,j,k)\right) = 2^{-3r},$$

its surface consists of at least six Jordan faces, and its surface area equals

$$J_{area}\left(\mathbf{C}_r(i,j,k)\right) = 6 \cdot 2^{-2r}.$$

In relation to the fixed coordinate scales of the reference space $\mathbf{R}^3$ we define $\mathbf{Z}^3_r$ to be the *r-grid point set* where each r-grid point (i,j,k) is the midpoint of the cell $\mathbf{C}_r(i,j,k)$:

Definition 5 (Grid Point Set of Specified Resolution): The *r-grid point structure* $\left[\mathbf{Z}^3, \xi_r\right]$ consists of the base set $\mathbf{Z}^3$ of all grid points in 3D, and an *interpretation* ξ_r which maps an r-grid point (i,j,k) into $\mathbf{R}^3$, onto the midpoint of the cell $\mathbf{C}_r(i,j,k)$, for $r = 0,1,2,....$ Let $\mathbf{Z}^3_r = \left\{\xi_r(\mathbf{p}) : \quad \mathbf{p} \in \mathbf{Z}^3\right\}$.

It follows that $\mathbf{Z}_r = \{m \cdot 2^{-r} : m \in \mathbf{Z}\}$. An r-grid point $\mathbf{p}$ may be specified by its *name* $(i,j,k) \in \mathbf{Z}^3$ or by its geometrical location $\xi_r(\mathbf{p})$. This dual approach allows the discussion of general grid terminology as neighborhoods or connectedness on the base of names of r-grid points in $\mathbf{Z}^3$, and geometric properties of refined grids on the base of their geometric interpretations in $\mathbf{Z}_r^3$.

All $N_r \times N_r \times N_r$ r-grid points $\mathbf{p} = (i,j,k)$ correspond to a finite subset of the infinite base set $\mathbf{Z}^3$. Assuming that the overall geometrically represented cube in $\mathbf{R}^3$, the *universe*

$$\mathbf{C}_{universe} = \{(x,y,z) \in \mathbf{R}^3 : 0 \le x,y,z \le N_0 + 1\}$$

is constant for a certain image analysis situation it follows that a larger resolution parameter r means a larger resolution $N_r = 2^r \cdot (N_0 + 1) - 1$, and vice versa.

Grid point spaces may be defined based on such a specified r-grid point structure, and these spaces are fundamental for multi-dimensional image analysis problems, see [24] and [32]. Neighborhood relations are introduced on the base set $\mathbf{Z}^3$ to specify adjacency or connectedness properties. For $0 \le t \le 2$ and $t \in \mathbf{Z}$, let

$$fix_t = \{(x_1, x_2, x_3) : \forall i (1 \le i \le 3 \rightarrow x_i \in \{-1, 0, +1\}) \wedge card\{i : x_i = 0\} = t\}$$

be a subset of the surface of a three-dimensional cube $[-1,+1]^3$. For example, $(1,0,1) \in fix_1$ is in the surface but not a corner of this cube, and $fix_0 = \{-1,+1\}^3$ represents the set of all corners of this cube. Assuming that any *grid point* $\mathbf{p} \in \mathbf{Z}^3$ also denotes a *grid vector*, from the origin to the grid point $\mathbf{p}$, it follows that the addition of two grid points is uniquely defined.

Definition 6 (Neighborhood and Adjacency of Grid Points): For $\mathbf{p} \in \mathbf{Z}^3$ and $0 \le t \le 2$, the set

$$\eta_t(\mathbf{p}) = \mathbf{p} + \bigcup_{j=t}^{2} fix_j$$

denotes the *t-neighborhood* of point $\mathbf{p}$. For $\mathbf{q} \in \eta_t(\mathbf{p})$ we say that $\mathbf{q}$ is a *t-neighbor* of $\mathbf{p}$, and that $\mathbf{p}$ and $\mathbf{q}$ are *t-adjacent*.

The relation of t-adjacency is irreflexive and symmetric. The transitive closure of this relation defines *t-connectedness* for sets of grid points in 3D. For $\mathbf{p} \in \mathbf{Z}^3$ and $0 \le t \le 2$ we have

$$card(\eta_t(\mathbf{p})) = \sum_{j=t}^{2} 2^{3-j} \binom{3}{j},$$

i.e. $card(\eta_2(\mathbf{p})) = 6$, $card(\eta_1(\mathbf{p})) = 18$, and $card(\eta_0(\mathbf{p})) = 26$, accordingly the notions "6-, 18-, or 26-neighborhood" or "6-, 18-, or 26-connectedness" are common in digital 3D image analysis. A *homogeneous grid point net* $[\mathbf{Z}^3, \eta_t]$ can be defined, representing an infinite undirected labeled graph, with vertex set $\mathbf{Z}^3$ and edge set $\{(\mathbf{p},\mathbf{q}) : \mathbf{p} \in \mathbf{Z}^3 \wedge \mathbf{q} \in \eta_t(\mathbf{p})\}$. Nets of grid points are studied in [31]. The *homogeneous net of r-grid points* $[\mathbf{Z}^3, \eta_t, \xi_r]$ is also characterized by the interpretation ξ_r.

2.2 Digitization Schemes

A digitization mapping can be specified as a model of the given physical image acquisition process. This allows the use of real-world test objects for evaluation. The exact modeling of imaging processes such as confocal microscopy or MRI is a complex task, and evaluations based on statistical data (i.e. populations of test objects, e.g. calibration spheres [3]) are proper techniques to achieve meaningful results. We will not follow that way in this paper. Each image acquisition process (MRI, confocal microscopy etc.) would need its own specification. We prefer a more general approach.

A general digitization model specifies a certain mapping of given planes, straight lines, Jordan bodies, etc. contained in the universal cube $\mathbf{C}_{universe}$, into an orthogonal grid of size $N_r \times N_r \times N_r$. See for example [9] for a general scheme to define such models for m-dimensional spaces but without modeling refined resolutions.

A common (but in relation to hardware devices, idealized) model for digitizing oriented real arcs in $\mathbf{R}^2$ into the grid $\mathbf{Z}_r^2$ may be described as follows (the so-called *grid intersection digitization* [13, 23]). For any intersection point of arc γ with a grid line defined by two points (i, j_1), (i, j_2) or (i_1, j), (i_2, j) in $\mathbf{Z}_r^2$ the closest (according to Euclidean metric) grid point in $\mathbf{Z}_r^2$ to this intersection point in $\mathbf{R}^2$ will be chosen as an element of the digital image of γ; if the intersection point is the midpoint of a grid edge then the point on the right side of γ (according to its orientation) is chosen. In [7] a similar grid intersection scheme was used for the digitization of straight lines in $\mathbf{R}^3$.

Using this intersection scheme, the straight line (orientation with increase of parameter a)

$$\gamma = \{(a, 2^{-(r+1)} + a) : a \in \mathbf{R}\}$$

in $\mathbf{R}^2$ will always, for any $r \geq 0$, lead to the digital image $\mathbf{A}_r = \{(q,q) : q \in \mathbf{Z}_r\}$, for example. If in the case where the intersection point is a midpoint of a grid edge the point on the left side of γ is chosen, then the digital image $\mathbf{B}_r = \{(q,q+1) : q \in \mathbf{Z}_r\}$ would be the digitization result. If in this midpoint case the point closest to the origin is chosen the digital image $\mathbf{A}_r \cup \mathbf{B}_r$ would result.

We return to the 3D case. To avoid such "midpoint discussions" for curves in 3D it can be suggested that we assume for arcs γ in $\mathbf{R}^3$ that for any crossing with a grid plane $x_i = q \in \mathbf{Z}_r$ at point $\mathbf{p}$ there is exactly one grid point in $\mathbf{Z}_r^3$ that is the closest grid point to $\mathbf{p}$, for any coordinate axis $1 \leq i \leq 3$. This assumption is violated only by a set of measure zero assuming a straightforward defined measurable space of all arcs in 3D.

Let Π_r^σ be a bounded subset of $\mathbf{R}^3$ containing at least the origin of $\mathbf{R}^3$, for $r = 1,2,3,...$ and σ is a metavariable of a name of the given set. Examples for such sets Π_r^σ are

$$\Pi_r^{cube} = \left\{(x_1, x_2, x_3) : \quad \max_{1 \leq i \leq 3} |x_i| \leq 2^{-r}\right\},$$

$$\Pi_r^{octahedron} = \left\{(x_1, x_2, x_3) : \quad \max\left\{|x_1|, |x_2|, |x_3|, \tfrac{1}{2}\sum_{i=1}^{3} |x_i|\right\} \leq 2^{-r}\right\},$$

$$\Pi_r^{sphere} = \left\{(x_1, x_2, x_3) : \quad \sum_{i=1}^{3} x_i^2 \leq 2^{-2r}\right\}, \text{ and}$$

$$\Pi_r^{cross} = \left\{(x_1, x_2, x_3) : \quad \max_{1 \leq i \leq 3} |x_i| \leq 2^{-r} \wedge \exists j\left(1 \leq j \leq m \wedge x_j = 0\right)\right\},$$

for $r = 1,2,3,....$

Let $\Pi_r^\sigma(\mathbf{q}) = \{\mathbf{q} + \mathbf{p} : \mathbf{p} \in \Pi_r^\sigma\} = \mathbf{q} + \Pi_r^\sigma$ for any point $\mathbf{q} \in \mathbf{R}^3$. For any r-grid point $\mathbf{p} = \left(i \cdot 2^{-r}, j \cdot 2^{-r}, k \cdot 2^{-r}\right) \in \mathbf{Z}_r^3$ and $\sigma \in \{octahedron, sphere, cross\}$ it holds that

$$\Pi_r^{cube}(\mathbf{p}) = \mathbf{C}_{r-1}(i,j,k),$$

and the sets $\Pi_r^\sigma(\mathbf{p})$ are subsets of the cell $\mathbf{C}_{r-1}(i,j,k)$.

Furthermore assume that Π_r^σ satisfies the following uniqueness condition that for each point $\mathbf{p} \in \mathbf{R}^3$ there exists at most one grid point $\mathbf{q} \in \mathbf{Z}_r^3$ such that $\mathbf{p} \in \Pi_r^\sigma(\mathbf{q})$. The given example sets satisfy these constraints. It holds that $\mathbf{q} \in \mathbf{Z}_r^3$ is exactly the only one r-grid point in $\Pi_r^\sigma(\mathbf{q})$. We use such a set Π_r^σ as the *domain of influenc*e of a digitization scheme, where σ specifies the name of the scheme.

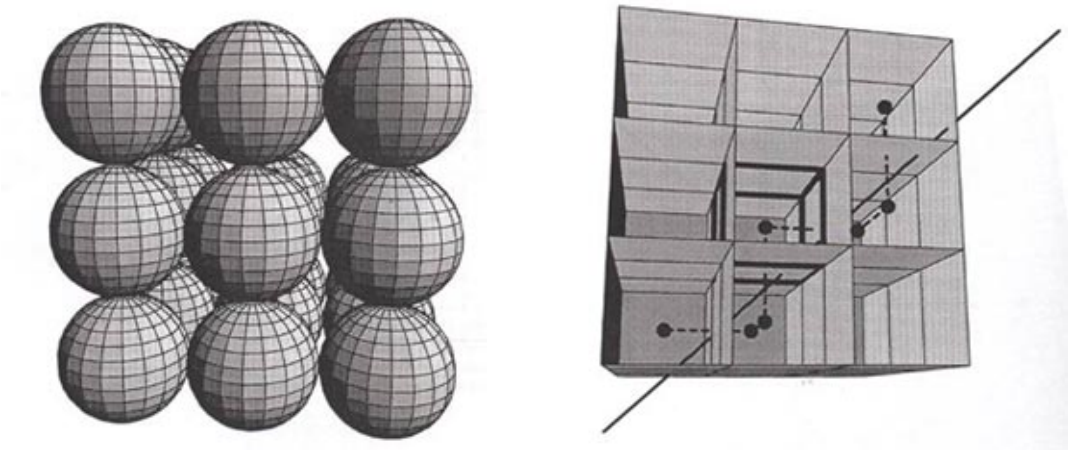

Figure 2 [4]**:** The generalization of 2D circle intersection digitization to 3D spherical digitization (on the left) allows that infinite straight lines can pass between the spheres without intersecting any of them. However the scheme can be considered for digitizing solid 3D objects. The cube intersection digitization (on the right) maps a straight line into a 6-connected grid-point sequence.

Definition 7 (Intersection Digitization): For $\mathbf{p} \in \mathbf{R}^3$, a name σ and $r = 1, 2, 3, \ldots$ let

$$DIG_r^{\sigma}(\mathbf{p}) = \begin{cases} \{\mathbf{q}\} & \text{if } \mathbf{q} \in \mathbf{Z}_r^3 \text{ and } \mathbf{p} \in \Pi_r^{\sigma}(\mathbf{q}) \\ \varnothing & \text{otherwise} \end{cases}.$$

For a subset Θ of $\mathbf{R}^3$,

$$DIG_r^{\sigma}(\Theta) = \bigcup_{\mathbf{p} \in \Theta} DIG_r^{\sigma}(\mathbf{p})$$

denotes the digital image of Θ according to the *intersection digitization* mapping DIG_r^{σ}.

Corollary 1: *An r-grid point $\mathbf{q} \in \mathbf{Z}_r^3$ is in the digital image $DIG_r^{\sigma}(\Theta)$ of a set $\Theta \subseteq \mathbf{R}^3$ iff $\Theta \cap \Pi_r^{\sigma}(\mathbf{q}) \neq \varnothing$.*

The different domains of influence define intersection digitization schemes as DIG_r^{cube}, $DIG_r^{octahedron}$, DIG_r^{sphere}, or DIG_r^{cross}.

The scheme DIG_r^{cross} is the *grid-intersection digitization* in 3D. In [4] it is shown that grid-intersection digitization is "a poor choice" for digital curve representation in 3D space and that cube quantization, which leads to 6-connected r-grid points in $\mathbf{Z}_r^3$, should be preferred. The sphere intersection

digitization scheme is not suitable for curves since even infinite straight lines can pass between the spheres without intersecting any of them, see Fig. 2.

However for digitizing Jordan bodies Θ the use of such intersection digitization schemes may be suggested for consideration. An intersection digitization of a Jordan body Θ leads to a certain r-grid point set which may also be represented as a binary voxel data cube f.

Definition 8 (Inclusion Digitization): For a subset Θ of $\mathbf{R}^3$ and a domain of influence Π_r^σ,

$$dig_r^\sigma(\Theta) = \left\{ \mathbf{q} \in Z_r^3 : \quad \Pi_r^\sigma(\mathbf{q}) \subseteq I(\Theta) \right\}$$

denotes the digital image of Θ according to the *inclusion digitization* mapping dig_r^σ.

Examples of inclusion digitization mappings are dig_r^{cube}, $dig_r^{octahedron}$, dig_r^{sphere}, and dig_r^{cross}. The assumed properties of areas of influence lead to the following

Corollary 2: *For any set* $\Theta \subset \mathbf{R}^3$ *and any domain of influence* Π_r^σ *it holds that* $dig_r^\sigma(\Theta) \subseteq \Theta \cap \mathbf{Z}_r^3 \subseteq DIG_r^\sigma(\Theta)$.

F. Sloboda [28] suggests using DIG_r^{cube} to define an *outer interior* $\mathbf{I}_r^+ = I_r^+(\Theta)$, and dig_r^{cube} to define an *inner interior* $\mathbf{I}_r^- = I_r^-(\Theta)$ of a Jordan body Θ. Let

$$body_r(\mathbf{G}) = \bigcup_{\mathbf{q} \in \mathbf{G}} \Pi_{r+1}^{cube}(\mathbf{q})$$

where $\mathbf{G}$ denotes a set (of geometric locations) of r-grid points in $\mathbf{Z}_r^3$, and $r = 0,1,2,\ldots$. The general definition utilizing arbitrary domains of influence is as follows:

Definition 9 (Inner, Intermediate and Outer Interior): For a subset Θ of $\mathbf{R}^3$ and a domain of influence Π_r^σ,

$$\mathbf{I}_r^{\sigma-} = I_r^{\sigma-}(\Theta) = body_r\left(dig_r^\sigma(\Theta)\right) \text{ and } \mathbf{I}_r^{\sigma+} = I_r^{\sigma+}(\Theta) = body_r\left(DIG_r^\sigma(\Theta)\right)$$

denote the *inner* and the *outer interior*, respectively, and

$$\mathbf{I}_r = I_r(\Theta) = body_r\left(\Theta \cap \mathbf{Z}_r^3\right)$$

denotes the *intermediate interior*.

The inner, intermediate, and outer exterior $\mathbf{E}_r^{\sigma-}$, $\mathbf{E}_r$, and $\mathbf{E}_r^{\sigma+}$ could be defined in a similar way. - With Corollary 2 it follows immediately that also these volume data satisfy the monotonicity property of

Corollary 3 [25]**:** *For any set* $\Theta \subset \mathbf{R}^3$ *and any domain of influence* Π_r^σ *it holds that* $I_r^{\sigma-}(\Theta) \subseteq I_r(\Theta) \subseteq I_r^{\sigma+}(\Theta)$.

It follows that

$$J_{volume}\left(I_r^{\sigma-}(\Theta)\right) = card\left(dig_r^\sigma(\Theta)\right) \cdot 2^{-3r},$$
$$J_{volume}\left(I_r(\Theta)\right) = card\left(\Theta \cap Z_r^3\right) \cdot 2^{-3r}, \text{ and}$$
$$J_{volume}\left(I_r^{\sigma+}(\Theta)\right) = card\left(DIG_r^\sigma(\Theta)\right) \cdot 2^{-3r}$$

are the volumes of these different discrete representations of the given set $\Theta \subset \mathbf{R}^3$, and the surface areas J_{area} of these different discrete representations may be calculated in a similar way adding all the surface areas of faces on the boundaries of the sets $I_r^{\sigma-}$, I_r, and $I_r^{\sigma+}$.

In the following we omit the domain of influence index σ if the discussion is about the *cube* digitization scheme, i.e. it is $dig_r = dig_r^{cube}$, $I_r^+ = I_r^{cube+}$ etc. in what follows.

Cube Digitization Theorem: *The proper inclusion* $\mathbf{I}_r^- \subset I\left(\mathbf{I}_r^+\right)$ *holds for any non-empty subset* Θ *of* $\mathbf{R}^3$.

It follows that $\partial\mathbf{I}_r^- \cap \partial\mathbf{I}_r^+ = \varnothing$. Note that the set $\mathbf{I}_r^-$ may be empty for a non-empty set Θ and a selected resolution r. But the set $\mathbf{I}_r^+$ will always be non-

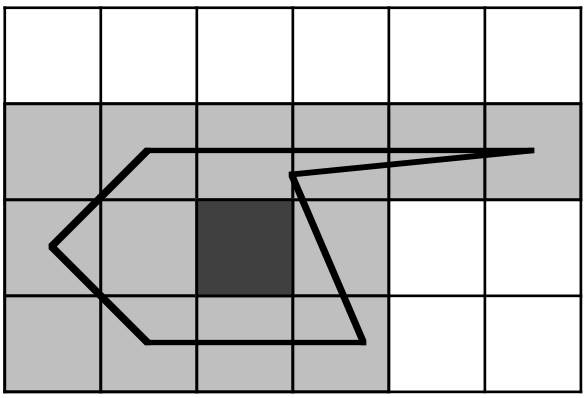

Figure 3: Cells in 2D showing the inner interior (one cell - dark shaded) and the outer interior (14 cells - light or dark shaded).

empty for a non-empty set Θ. Fig. 3 illustrates an example of *square* intersection digitization in 2D. Here the polygonal border of this polygon passes on the left exactly through the vertices of cells introducing some extra cells into the outer interior, and it also possesses a "thin spike" ("thin" with respect to the resolution!) on the right generating some cells for the outer interior which are further away from the inner interior. Similar situations may appear for *cube* intersection digitization in 3D.

3 Convergence Analysis

So far the necessary definitions were given for starting the analysis of such specific 3D image analysis problems as measuring the volume or the surface area of a digitized 3D object, approximating a connected region of given digital surface points by a special explicit face function as, e.g., a plane, calculating height data of an object face which is only given by gradient values at discrete locations, or discrete recovery of a Jordan face as a special solution of a Cauchy problem. The latter two problems are relevant to shape reconstruction, see [10]. The brief discussion of these four situations are different case studies of the general soundness approach if gridding techniques are applied.

3.1 Volume and Surface Area Calculation

We assume as input a finite 6-connected set $\mathbf{G} \subset \mathbf{Z}^3$ of grid points. This set is assumed to be a digital representation of a Jordan body Θ, for a certain resolution parameter r. Therefore it is assumed that $\mathbf{G}$ is geometrically interpreted to be an r-grid point set contained in $\mathbf{Z}_r^3$.

TASK: The task is to calculate the volume and the surface area of Θ based on the available input set $\mathbf{G} \subset \mathbf{Z}_r^3$.

What is methodologically a sound approach for calculating these features satisfying the soundness properties stated in Section 1.1?

The digitization process is modeled as being a *cube* intersection digitization method. Thus the given grid point set $\mathbf{G}$ is identified with an r-grid point representation $DIG_r(\Theta)$ of the unknown 3D object Θ, and this set defines the inner interior $\mathbf{I}_r^-$. Furthermore we can generate the smallest possible (which is uniquely defined, see the Cube Digitization Theorem above) outer interior $\mathbf{I}_r^+$ by a simple dilation operation on $\mathbf{G}$ using the 26-neighborhood as a structural element (dilation is defined and studied on the set $\mathbf{Z}^3$ of names of r-grid

points). This dilation leads to an expanded set $\mathbf{G}^+$ which may be considered to be the set $DIG_r(\Theta)$ which finally defines $\mathbf{I}_r^+$. Because the actual shape of set Θ in $\mathbf{R}^3$ is unknown we are not able to suggest an approximation of the intermediate interior $\mathbf{I}_r$.

The volume calculation for the unknown object Θ in $\mathbf{R}^3$ may be based on $J_{volume}\left(\mathbf{I}_r^-\right)$ as well as on $J_{volume}\left(\mathbf{I}_r^+\right)$, see [25]. Both approaches are sound (convergence and convergence towards proper value) for Jordan bodies Θ:

Volume Measurement Theorem: *For any Jordan body* $\Theta \subset \mathbf{R}^3$ *it holds that*

$$J_{volume}(\Theta) = \sup_{r\to 0} J_{volume}\left(\mathbf{I}_r^-\right) = \inf_{r\to 0} J_{volume}\left(\mathbf{I}_r^+\right),$$

where $\mathbf{G} = dig_r(\Theta)$, $\mathbf{I}_r^- = body_r(\mathbf{G})$, *and* $\mathbf{I}_r^+ = body_r\left(\mathbf{G}^+\right)$.

Unfortunately such a convergence $J_{volume}(\Theta) = \lim_{r\to 0} J_{volume}\left(\mathbf{I}_r^-\right) = \lim_{r\to 0} J_{volume}\left(\mathbf{I}_r^+\right)$ to the proper value is not true in general for the case of surface area measurement. However a sound measurement procedure for surface areas of Jordan bodies was developed in [28]. For explaining this approach we first note that both the inner interior $\mathbf{I}_r^- = body_r(\mathbf{G})$, and the outer interior $\mathbf{I}_r^+ = body_r\left(\mathbf{G}^+\right)$ are polyhedrons in $\mathbf{R}^3$, with $\mathbf{I}_r^- \subset I\left(\mathbf{I}_r^+\right)$ (see Cube Digitization Theorem).

Minimum Jordan Surface Theorem [28]**:** *Assume that* Π_1, Π_2 *are polyhedrons in* $\mathbf{R}^3$ *with* $\Pi_1 \subset I(\Pi_2)$. *Then there exists a uniquely defined Jordan surface* $\mathbf{S}$ *in* $\Pi_2 - I(\Pi_1)$ *with minimum surface area, which is the boundary of a certain polyhedron* Π.

The set $\Pi_2 - I(\Pi_1)$ is polyhedral bounded and compact. It follows that the *minimum Jordan surface* $\mathbf{S} = \partial\Pi$ "is between" the inner polyhedral surface $\partial\Pi_1$ and the outer polyhedral surface $\partial\Pi_2$, i.e. $\Pi_1 \subseteq \Pi \subset \Pi_2$.

Corollary 4: *There exists a uniquely defined minimum Jordan surface in the compact set* $body_r\left(\mathbf{G}^+\right) - I\left(body_r(\mathbf{G})\right)$.

Starting with a Jordan body Θ, the set $\mathbf{G}$ was defined by resolution r. Thus Θ and r uniquely define a minimum Jordan surface $MJS_r(\Theta)$ having a surface area of $J_{area}\left(MJS_r(\Theta)\right)$. An example is illustrated in Fig. 4.

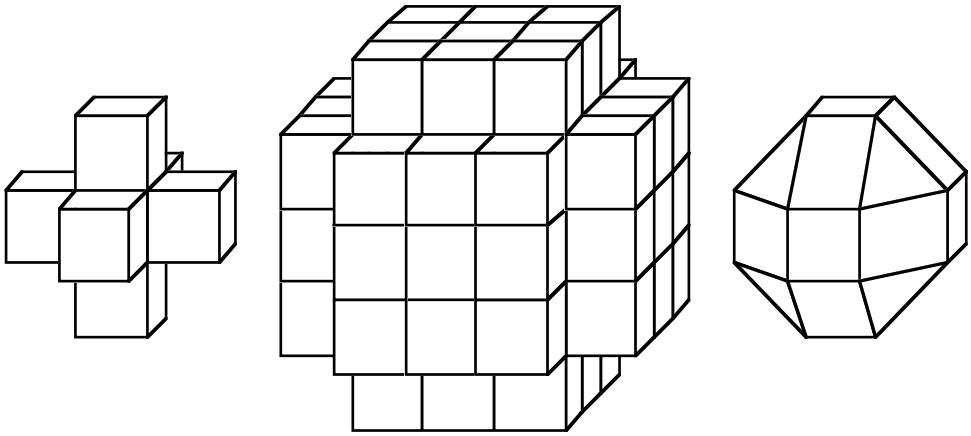

Figure 4 [28] **:** Example of an inner interior (on the left), an outer interior (middle), and a minimum Jordan surface (on the right).

Surface Measurement Theorem [28]**:** *For any Jordan body* $\Theta \subset \mathbf{R}^3$ *it holds that*

$$J_{area}(\partial\Theta) = \lim_{r\to\infty} J_{area}(MJS_r(\Theta))$$

where $MJS_r(\Theta)$ *is the uniquely defined minimum Jordan surface for resolution* $r = 0,1,2,\ldots$.

Altogether this specifies a sound (i.e. convergence and convergence towards the proper value) procedure for calculating the surface area of a digitized Jordan body. However the design of time-efficient algorithms for calculating the minimum Jordan surface polyhedron should be an interesting problem in computational geometry where a 6-connected grid point set is given as input. The 2D case of minimum perimeter polygons is treated in [27].

Marching cubes [18] may be considered to define an approximation technique for calculating minimum Jordan surfaces. Each elementary grid cube, defined by eight grid points, is treated according to a look-up table for defining planar surface patches within this elementary grid cube. See Fig. 5 for a complete set of marching cubes configurations as specified in [5]. The fourteen basic configurations originally suggested by [18] are incomplete. Occasionally they generate "surfaces with holes". The marching cubes algorithm determines the surface by deciding how the surface intersects a given elementary grid cube. A surface can intersect an elementary grid cube in 2^8 different ways, and these can be represented as fourteen major cases with respect to rotational symmetry.

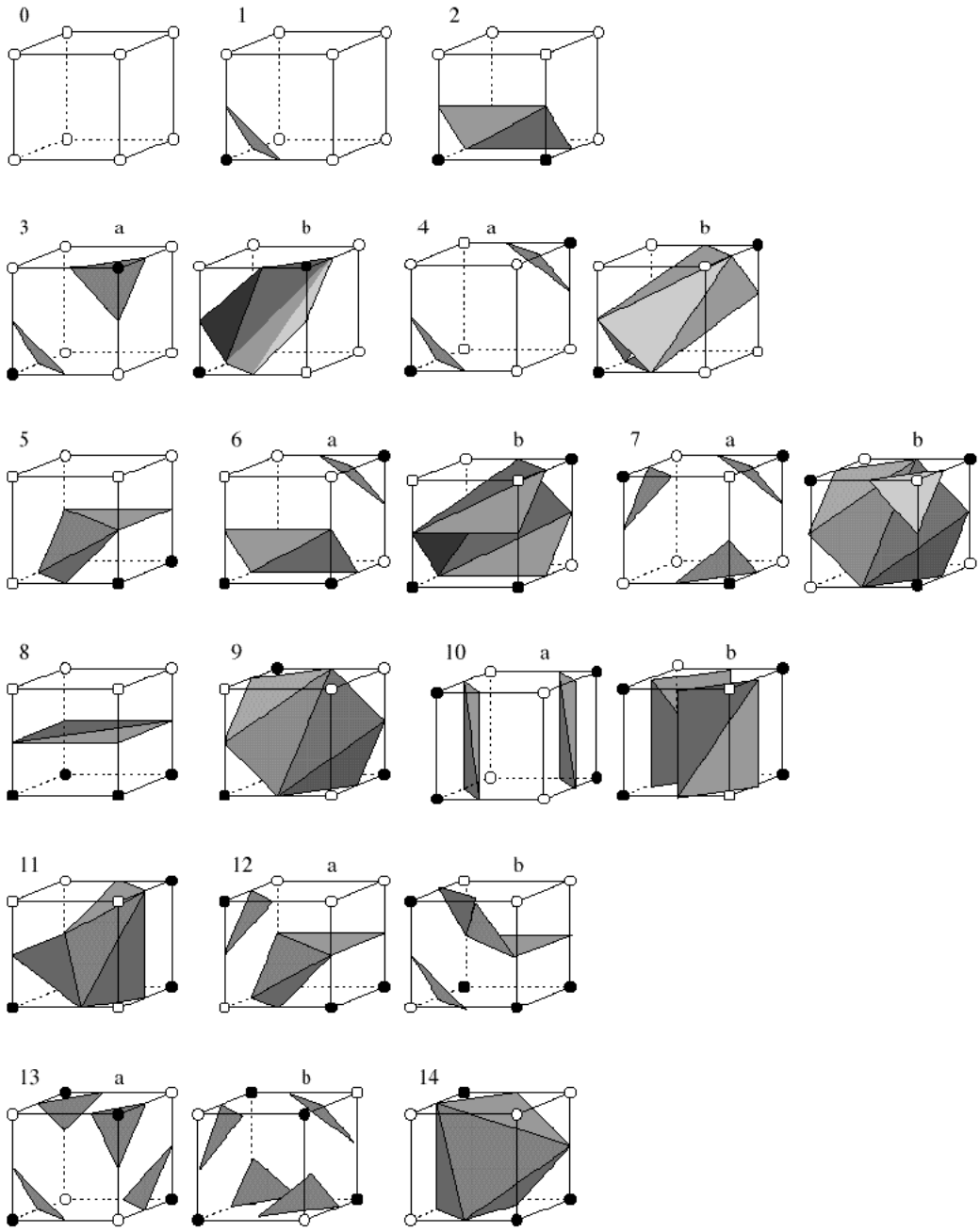

Figure 5 [5]**:** Basic cases for a marching cube algorithm.

Alternatively a method developed by [34] calculates the contour chains immediately without using a look-up table of all 2^8 different cases.

Disambiguities of the marching cube look-up tables are discussed in [33]. A marching tetrahedra algorithm was suggested in [22]. It generates more triangles than the marching cubes algorithm in general. Trilinear interpolation functions were used in [2] for the different basic cases of the marching cubes

algorithm. In comparison to the marching cube algorithm [5] the accuracy of the calculated surface area improved by using this trilinear marching cube algorithm, which was confirmed for a few synthetic Jordan faces.

3.2 Approximation of Planes

We assume as input a finite set $\mathbf{G} \subset \mathbf{Z}^3$ of grid points. This set is assumed to be a digital representation of a compact planar set Θ incident with a plane $\alpha \subset \mathbf{R}^3$. We assume that $\mathbf{G}$ is geometrically interpreted to be an r-grid point set contained in $\mathbf{Z}_r^3$. Concerning the digitization method assume that the plane α is digitized using an intersection digitization scheme DIG_r^{below} in which the first grid points "below the given plane" are taken, i.e. we translate the set Π_r^{cube} by $\left(0,0,\frac{1}{2}\right)$ half of a $\mathbf{Z}_r^3$ unit 2^{-r}, "open it" at the upper face, and the resulting set is Π_r^{below}. This digitization scheme is also equivalent to translating the plane by half of a $\mathbf{Z}_r^3$ unit towards the xy-plane and rounding off z-values with respect to this unit.

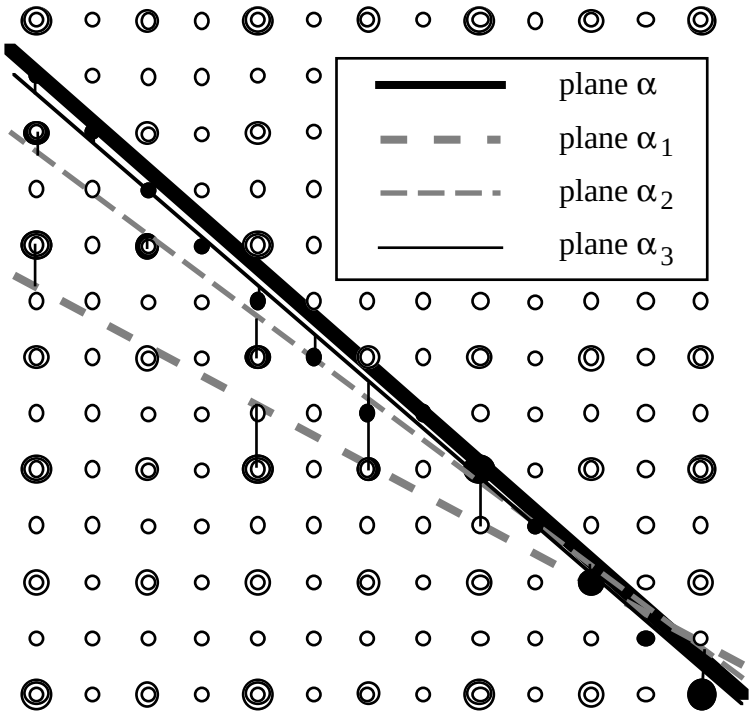

Figure 6: A 2D sketch of three consecutive approximations of a given plane. The lowest resolution produces a plane supported by four sampling points, the next resolution level is based on seven sampling points, and the third resolution level is based on 13 samples, all below or on the given plane. The approximation planes will intersect the given plane somewhere in general.

This digitization scheme defines a *digital plane* as an r-grid point set $DIG_r^{below}(\alpha) = \{(i,j,k) \in \mathbf{Z}_r^3 : k = \lfloor ai + bj + c \rfloor_r\}$ where $\lfloor u \rfloor_r$ is the greatest number in $\mathbf{Z}_r$ not larger than the real number u. This is arbitrary sparse as a plane approaches vertical.

<u>*TASK:*</u> A non-vertical plane α has to be determined in the explicit form $z = a_0 x + b_0 y + c_0$ from the finite input set $\mathbf{G} \subset \mathbf{Z}_r^3$.

The input set $\mathbf{G}_r = DIG_r^{below}(\Theta)$ is a finite subset of a digital plane. Of course there are different planes α which may generate a set $\mathbf{G}_r$ in this way. Therefore a solution specifying the unknown ground truth α is not possible if only one input set $\mathbf{G}_r$ is given. But still we may be able to solve this task by calculating a unique solution α_r which converges towards α as the resolution r increases, see Fig. 6. A distance measure on the set of all planes has to be defined for specifying convergence of planes. A convergent method for calculating such a sequence of planes α_r would be methodologically sound with respect to the soundness properties stated in Section 1.1. As a necessary condition the method should allow calculation of a unique solution α_r for given sets $\mathbf{G}_r$, for $r \geq r_0$. What is the minimum size of a set $\mathbf{G}_r$ which allows such a method?

The use of least-square approximation allows us to specify such a sound method for calculating these approximation planes based on discrete input data.

The use of a least-squares approximation techniques for representations of digital objects was proposed in [20]. In [21] it was proved that the *least-square approximation straight-line* uniquely determines the digital straight-line where the input data are given for a certain digital interval.

We define the *least-square approximation plane*

$$LSA_{plane}(\mathbf{G}_r)$$

for $\mathbf{G}_r$ to be a plane which minimizes the sum of the squares of the vertical distances to all points in $\mathbf{G}_r$. Note that this error measure is related to the assumed digitization model, and the resolution parameter r has impact on this measure by defining scaling and the sampling rate for the set Θ incident with α.

A method for determining such least-square approximation planes is well-known from statistics, see, e.g. [1], where a general, not necessary digital input $\{(x_i, y_i, z_i) : i = 1,2,...,t\}$ is assumed. A comparison with an unknown ground truth is not relevant in statistics, and a discussion of different resolutions is also irrelevant in this general case. For such a general case assume that the equation

of the least-square approximation plane $LSA_{plane}(\mathbf{G})$ is parameterized as $z = ax + by + c$. Then the error function

$$\Phi(\mathbf{G}; a, b, c) = \sum_{i=1}^{t} \left(ax_i + by_i + c - z_i \right)^2$$

has to be minimized. This traditional optimization problem is solved by obtaining the coefficients a, b, and c from the equation system

$$\frac{\partial \Phi}{\partial a} = 0, \ \frac{\partial \Phi}{\partial b} = 0, \text{ and } \frac{\partial \Phi}{\partial c} = 0$$

i.e.

$$a\sum_{i=1}^{t} x_i^2 + b\sum_{i=1}^{t} x_i y_i + c\sum_{i=1}^{t} x_i = \sum_{i=1}^{t} x_i z_i,$$

$$a\sum_{i=1}^{t} x_i y_i + b\sum_{i=1}^{t} y_i^2 + c\sum_{i=1}^{t} y_i = \sum_{i=1}^{t} y_i z_i, \text{ and}$$

$$a\sum_{i=1}^{t} x_i + b\sum_{i=1}^{t} y_i + c\sum_{i=1}^{t} 1 = \sum_{i=1}^{t} z_i.$$

A unique solution exists whenever the determinant of this equation system is not zero. For example, if all points in $\mathbf{G}$ coincide with a straight line then the solution is not unique.

The special case of a digital input set $\mathbf{G}_r$ was studied in [11]. An r-grid point set $\mathbf{G}_r \subset \mathbf{Z}_r^3$ is a *digital quadrangle* if there exists a plane α in $\mathbf{R}^3$ and integers m and n such that

$$\mathbf{G}_r = \left\{ (i, j, k) : i \in \left\{ h2^{-r} : 1 \le h \le m \right\} \wedge j \in \left\{ h2^{-r} : 1 \le h \le n \right\} \wedge k = \lfloor ai + bj + c \rfloor_r \right\}.$$

The *projection* $proj_{1,2}(\mathbf{G}_r)$ of a digital quadrangle into the ij-plane is a rectangular set of r-grid points. As for Θ in general, there are different planes α satisfying this equation for a given digital quadrangle.

The coefficients

$$\sum_{i=1}^{t} 1, \ \sum_{i=1}^{t} x_i, \ \sum_{i=1}^{t} y_i, \ \sum_{i=1}^{t} x_i^2, \ \sum_{i=1}^{t} y_i^2, \text{ and } \sum_{i=1}^{t} x_i y_i$$

of the general equation system can easily be calculated for the assumed input of a digital quadrangle. Let

$$M_{ab}(\mathbf{G}_r) = \sum_{(i,j,k(i,j))\in\mathbf{G}_r} i^a \cdot j^b \cdot k(i,j)$$

be the *moment of order ab* of the set $\mathbf{G}_r$. This leads to a special form of this equation system:

$$\frac{nm(m-1)(2m-1)}{6}\cdot a + \frac{nm(n-1)(m-1)}{4}\cdot b + \frac{nm(m-1)}{2}\cdot c = M_{10}(\mathbf{G}_r),$$

$$\frac{nm(n-1)(m-1)}{4}\cdot a + \frac{nm(2n-1)(n-1)}{6}\cdot b + \frac{nm(n-1)}{2}\cdot c = M_{01}(\mathbf{G}_r), \text{ and}$$

$$\frac{nm(m-1)}{2}\cdot a + \frac{nm(n-1)}{2}\cdot b + nm\cdot c = M_{00}(\mathbf{G}_r).$$

This system has a determinant equal to

$$(n^2-1)(m^2-1)n^3m^3/144,$$

and so, for $n>1$ and $m>1$ the coefficients a, b, and c are uniquely determined.

LSA Uniqueness Theorem [11]**:** *Let* $\mathbf{G}_r \subset Z_r^3$, $\mathbf{H}_r \subset Z_r^3$, *with* $proj_{1,2}(\mathbf{G}_r) = proj_{1,2}(\mathbf{H}_r)$. *Assume that both sets contain at least one* 2×2 *digital quadrangle, and let* $LSA_{plane}(\mathbf{G}_r)$ *and* $LSA_{plane}(\mathbf{H}_r)$ *be the corresponding least-square approximation planes. Then it holds that* $\mathbf{G}_r = \mathbf{H}_r$ *iff* $LSA_{plane}(\mathbf{G}_r) = LSA_{plane}(\mathbf{H}_r)$.

This result allows us to define storage-efficient representations (coding schemes) for digital plane segments. In the context of this paper it also supports a possible way to analyze the soundness of the least-squares approximation approach.

As a corollary of *Blichfeldt's theorem*, see [25], it follows that for a given non-trivial compact set Θ incident with a plane α it holds that for $r \geq r_0$, any input set $\mathbf{G}_r = DIG_r^{below}(\Theta)$ always contains at least a 2×2 digital quadrangle. Thus it holds that for $r \geq r_0$ the set $\mathbf{G}_r$ uniquely determines a plane $\alpha(\mathbf{G}_r) = \alpha_r$ with representation $z = a_r x + b_r y + c_r$. The plane α is assumed to be specified by $z = a_0 x + b_0 y + c_0$. We define the distance between such two planes by

$$d_{plane}(\alpha(\mathbf{G}_r), \alpha) = \sqrt{(a_r - a_0)^2 + (b_r - b_0)^2 + (c_r - c_0)^2}\,.$$

This measure d_{plane} is a metric on the set of all planes in $\mathbf{R}^3$.

LSA Convergence Theorem: *Let* $\mathbf{G}_r = DIG_r^{below}(\Theta)$ *for a compact set* Θ *incident with a plane* α. *Assume that* $\mathbf{G}_{r_0}$ *contains a* 2×2 *digital quadrangle. Then* $d_{plane}(\alpha(\mathbf{G}_r), \alpha)$ *is defined for* $r \geq r_0$, *and it follows that*

$$\lim_{r \to \infty} \quad d_{plane}(\alpha, \alpha(\mathbf{G}_r)) = 0 .$$

This convergence theorem concludes the soundness proof for the specified least-square approximation technique for reconstructing a plane in 3D. It is conjectured that even the following monotonicity property

$$d_{plane}(\alpha, \alpha(\mathbf{G}_{r+1})) \leq d_{plane}(\alpha, \alpha(\mathbf{G}_r))$$

holds, for $r \geq r_0$. There are cases where $d_{plane}(\alpha, \alpha(\mathbf{G}_{r+1})) = d_{plane}(\alpha, \alpha(\mathbf{G}_r))$, see for example a plane α parallel to the xy-plane defined by $z = const \cdot 2^{-r_1}$ where *const* is an integer.

3.3 Integration of Jordan Face Gradients

We assume as input a finite set $\mathbf{P}_r$ of gradients $(p(x,y), q(x,y))^T \in \mathbf{R}^2$ at exactly all r-grid point positions in the interior of the base set

$$proj_{1,2}(\mathbf{C}_{universe}) = \{(x,y) \in \mathbf{R}^2 : 0 \leq x, y \leq N_0 + 1\}$$

of the universal cube $\mathbf{C}_{universe}$. This set is assumed to be a digital representation of one (!) measurable Jordan face $\mathbf{F} = \mathbf{F}_{\mathbf{B}}(\varphi, \psi, \chi)$, for a certain resolution parameter r. For the sequence of finite grids $I(\mathbf{B}) \cap \mathbf{Z}_r^3$ it holds that

$$\lim_{r \to \infty} (I(\mathbf{B}) \cap \mathbf{Z}_r^3)$$

is dense in $\mathbf{B}$. W.l.o.g., let $\mathbf{B} = proj_{1,2}(\mathbf{C}_{universe})$, $x = \varphi(x,y)$, $y = \psi(x,y)$, and $z = \chi(x,y)$, i.e. the face is assumed to be in a position that allows a unique representation with respect to the xy-plane. It follows that

$$p(x,y) = \chi_x(x,y) = \tfrac{\partial \chi(x,y)}{\partial x} \text{ and } q(x,y) = \chi_y(x,y) = \tfrac{\partial \chi(x,y)}{\partial y}.$$

The assumed input situation corresponds to a certain step in *shading based shape recovery*, see, e.g., [10], when at first gradients are calculated based on given radiance information, and surface recovery has still to be performed based on this intermediate gradient information. For this case the open set $I(\mathbf{B})$ may be considered to be the *image domain* in the projection plane, and $z = \chi(x,y)$ denotes the *depth* of the surface points (roughly: the distance

between the camera and the projected object surface) assuming *parallel projection* as the model of the image acquisition process.

TASK: The task is to calculate the face **F** based on the available input set $\mathbf{P}_r$ of gradients at r-grid point positions.

Integration is uniquely determined up to an additive constant what corresponds to a translation of function χ, i.e. only a *main function* χ_0 may be calculated with $z = \chi_0(x,y) + const$, but the global additive parameter *const* remains unknown. Thus the task is actually that a differentiable main function χ_0 has to be calculated, and *const*, a global "shift in depth", can not be specified. In computer vision applications, this value *const* can be estimated by triangulation techniques (a pair of corresponding points in binocular stereo images, a surface point illuminated by a laser point light source, etc.). Also note that we are not able to calculate explicit representations of an unknown face **F** in general. The face **F** can be the "visible surface of an scene object of arbitrary complexity". The goal is to generate all χ_0 values at all r-grid points in the open base set $I(\mathbf{B})$.

After this specification of the task, we first have to determine for which Jordan surfaces this problem of calculating χ_0 values based on gradient information is uniquely solvable. As a corollary of *Frobenius' Theorem* it holds that the *integrability condition*

$$p_y(x,y) = q_x(x,y)$$

has to be satisfied on **B** for the given vector field of gradients:

Face Integrability Theorem: *Let* $\left(p(x,y), q(x,y)\right)^T$ *be a* $C^{(1)}(\mathbf{B})$*-continuous vector field. Then there exists a* $C^{(2)}(\mathbf{B})$*-continuous main function* $\chi(x,y)$ *with* $\chi_x = p$ *and* $\chi_y = q$ *on* **B** *iff* χ *satisfies the integrability condition on* **B**.

For example, the *Schwarz function*

$$\chi(x,y) = \begin{cases} \frac{xy\left(x^2 - y^2\right)}{x^2 + y^2}, & \text{if} \quad (x,y) \neq (0,0) \\ \\ 0 \quad , & \text{if} \quad (x,y) = (0,0) \end{cases}$$

does not satisfy the integrability condition in point $(0,0)$. Furthermore there are functions which satisfy the integrability condition, but which are not $C^{(2)}$-

continuous [10]. The measurable Jordan face $\mathbf{F} = \mathbf{F}_{\mathbf{B}}(\chi)$ is defined to be *integrable* if χ is $C^{(2)}(\mathbf{B})$-continuous.

Now let γ be a piecewise $C^{(1)}$ curve in the set $\mathbf{B}$,

$$\gamma\colon \ [a,b] \to \Re^2, \text{ and } \gamma(t) = (\gamma_1(t), \gamma_2(t)) = (x(t), y(t))$$

with $a < b$, $\gamma(a) = (x_0, y_0)$ and $\gamma(b) = (\bar{x}, \bar{y})$. For any curve of this kind and any integrable face $\mathbf{F}$ it holds that

$$\chi(\bar{x}, \bar{y}) = \chi(x_0, y_0) + \int_{\gamma} p(x,y)\,dx + q(x,y)\,dy$$

$$= \chi(x_0, y_0) + \int_a^b \left[p(\gamma_1(t), \gamma_2(t)) \cdot \dot{\gamma}_1(t) + q(\gamma_1(t), \gamma_2(t)) \cdot \dot{\gamma}_2(t) \right] dt,$$

i.e. the result of the face function χ at position $(\bar{x}, \bar{y})$ is independent of the chosen curve γ. However the chosen initial value $\chi(x_0, y_0)$ has influence.

Now we consider the digital case. The gradient values of face $\mathbf{F}$ are assumed to be given for grid point positions. Assume that for $r \geq 0$ the digital path

$$\mathbf{g}_r = \left[(x_1, y_1), (x_2, y_2), \ldots, \left(x_{\left(2^r(N_0+1)-1\right)^2}, y_{\left(2^r(N_0+1)-1\right)^2} \right) \right]$$

is a repetition free 4-connected path passing through exactly all $N_r \times N_r$ r-grid points in the open base set $I(\mathbf{B})$. For consecutive grid points (x_{t-1}, y_{t-1}), (x_t, y_t) in this path $\mathbf{g}_r$, for $2 \leq t \leq \left(2^r(N_0+1)-1\right)^2$, it is

$$\text{either } dx_t = 2^{-r} \text{ and } dy_t = 0, \text{ or } dx_t = 0 \text{ and } dy_t = 2^{-r},$$

where $x_t = x_{t-1} + dx_t$ and $y_t = y_{t-1} + dy_t$. Such a path may follow a certain general generation scheme, e.g., to be a meander, a Peano, or a Hilbert scan [26]. A digital path $\mathbf{g}_r$ may be considered to be a *digital sample* of a piecewise $C^{(1)}$ curve γ_r in the set $\mathbf{B}$, i.e. the curve γ_r passes through all points listed in the digital path $\mathbf{g}_r$, i.e. through all r-grid points in the open base set $I(\mathbf{B})$ in a certain order. W.l.o.g. we assume that $\mathbf{g}_r$ always starts at

$$(x_1, y_1) = (2^{-r}, 2^{-r})$$

and ends at, say

$$\left(x_{\left(2^r(N_0+1)-1\right)^2}, y_{\left(2^r(N_0+1)-1\right)^2} \right) = (N_0 + 1 - 2^{-r}, N_0 + 1 - 2^{-r}).$$

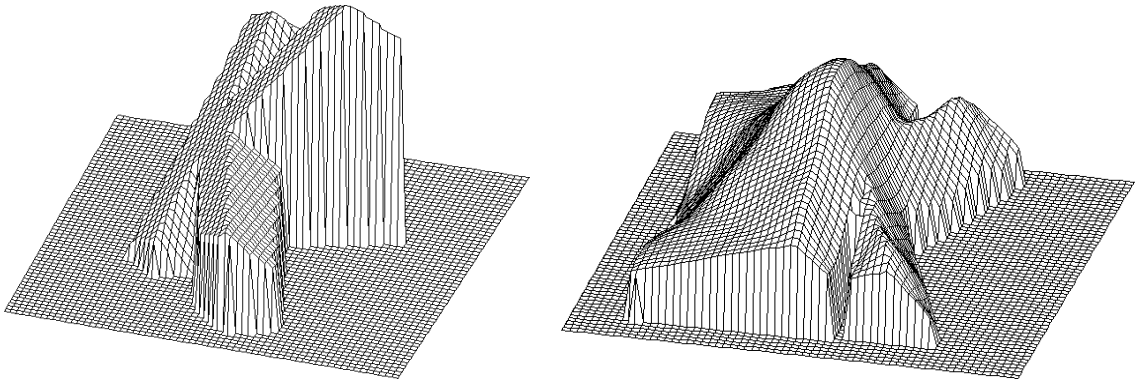

Figure 7 [12]**:** A K-shaped synthetic polyhedron with a maximum height of 162.43 grid units (on the left). The maximum height error of the reconstructed surface (on the right) is equal to 90.94 grid units where the visualized height values are averages of four different discrete path integrations (i.e. integrations following four different digital paths).

This allows γ_r to start at $\gamma_r(a)=(0,0)$ in "one corner" of the base set **B**, and leading to the diagonal corner $\gamma_r(b)=(N_0+1,N_0+1)$. We assume that $z_0=\chi(0,0)$ is given and take this value as a universal initial depth value for the *discrete path integration*

$$\chi_r(x_s,y_s)=z_0+\sum_{t=1}^{s}\left(p(x_t,y_t)\,dx_t+q(x,y)\,dy_t\right)$$

where point $(x_0,y_0)=(0,0)$ is assumed to be the start point of the path $\mathbf{g}_r$ for defining the initial step values dx_0 and dy_0.

Discrete Path Integration Theorem: *Let* $\mathbf{F}=\mathbf{F_B}(\chi)$ *be an integrable face and* **p** *be a point in the open base set* $I(\mathbf{B})$. *Then for any* $\varepsilon>0$ *there exists an integer* r_ε *and an* r_ε*-grid point* $\mathbf{p}_\varepsilon$ *in* $I(\mathbf{B})$ *such that* $\left|\chi(\mathbf{p})-\chi_r(\mathbf{p}_r)\right|<\varepsilon$.

This theorem points out that the specified discrete path integration method is sound with respect to convergence and convergence towards the proper value. The specific choice of the digital path γ_r is not important for proving this theorem, and this means that discrete path integration may start at different r-grid points, and may follow different path generation schemes as long as the initial value $\chi(x_0,y_0)$ is correct.

However for practical applications further soundness properties are of interest, as robustness with respect to noise, or with respect to "steep gradients" ("steep" in relation to the resolution r), see [12]. In this paper it was shown that the discussed discrete path integration technique has drawbacks if the face

$\mathbf{F} = \mathbf{F_B}(\chi)$ is more characterized by being a Jordan surface consisting of several planar faces (a "polyhedral object") instead of being a single integrable face, see Fig. 7. Of course, this corresponds to the Face Integrability Theorem as cited above.

3.4 Solution of a Cauchy Problem

As a final example for discussing the stated soundness properties of geometric algorithms based on gridding techniques we consider a special Cauchy problem. We assume as discrete input a collection of image data $E(x,y)$ at exactly all r-grid point positions in the interior $I(\mathbf{B})$ of the base set of the universal cube $\mathbf{C}_{universe}$. These image intensities are assumed to correspond to reflectance properties of the projected object surfaces according to a certain reflectance model. Assuming a linear reflectance model this leads to the (transformed) *linear image irradiance equation*

$$a\frac{\partial \chi}{\partial x}(x,y) + b\frac{\partial \chi}{\partial y}(x,y) = E(x,y),$$

which was studied in [14, 15]. As in Section 3.3 before we assume a measurable Jordan face $\mathbf{F} = \mathbf{F_B}(\chi)$ defined on set $\mathbf{B}$ where the values of the depth function χ are assumed to be known at some boundary points of $\mathbf{B}$ (*boundary condition*). The function E is assumed to be integrable on $\mathbf{B}$, and let $(a,b) \neq (0,0)$.

<u>*TASK:*</u> The task is to calculate the face $\mathbf{F}$ based on the available input set of irradiance values $E(x,y)$ at r-grid point positions, and based on a specified boundary condition, where the face satisfies the linear image irradiance equation.

More precisely, we are interested in a numerical solution of the following *Cauchy problem*: The face function χ is assumed to be integrable on base set $\mathbf{B}$. If $\text{sgn}(ab) \geq 0$ then

$$\chi(x,0) = f(x), \text{ for } 0 \leq x \leq N_0 + 1$$

is given as boundary condition, and if $\text{sgn}(ab) < 0$ then

$$\chi(x, N_0 + 1) = f(x), \text{ for } 0 \leq x \leq N_0 + 1$$

is given. Furthermore also

$$\chi(0,y) = g(y), \text{ for } 0 \leq y \leq N_0 + 1$$

is assumed to be known. The functions f, g are integrable on $[0, N_0+1]$ and satisfy $f(0)=g(0)$ if $\text{sgn}(ab)\geq 0$, or $f(0)=g(N_0+1)$ if $\text{sgn}(ab)<0$.

This Cauchy problem is given in "digital form", i.e. only values at r-grid point positions are given for functions $p=\chi_x$, $q=\chi_y$, E, f, and g.

For solving linear partial differential equations with the aid of the finite difference method see [30, Chapter 1]. As mentioned before in Section 3.3 it holds that

$$\lim_{r\to\infty}\left(I(\mathbf{B})\cap\mathbf{Z}_r^3\right)$$

is dense in $\mathbf{B}$. Assuming normed function spaces on $\mathbf{B}$ this sequence of grids allows us to define corresponding normed grid spaces, defined on subsets of $\mathbf{B}\cap\mathbf{Z}_r^3$, for functions defined on r-grid points, see [14, 15] for details. A *finite difference scheme* (FDS) is defined for all grids $\mathbf{B}\cap\mathbf{Z}_r^3$ of different resolution, for $r=0,1,2,...$, and basically it characterizes an operator R_r mapping an unknown function defined on $\mathbf{B}$, as χ in our case, into a function χ_r,

$$R_r(\chi)=\chi_r \text{ , with } \chi_r(i,j)\approx\chi\left(i\cdot 2^{-r}, j\cdot 2^{-r}\right)$$

defined on r-grid points which is considered to be an approximation of the unknown function.

For example, applying a (simple) *forward difference approach* together with Taylor's expansion yields

$$\left.\frac{\partial\chi}{\partial x}\right|_r^{(i,j)}=\frac{\chi_r(i+1,j)-\chi(i,j)}{2^{-r}}+O\left(2^{-r}\right)$$

in the x-direction, and

$$\left.\frac{\partial\chi}{\partial y}\right|_r^{(i,j)}=\frac{\chi_r(i,j+1)-\chi(i,j)}{2^{-r}}+O\left(2^{-r}\right)$$

in the y-direction. A (simple) *backward difference approach* in x-direction is given by

$$\left.\frac{\partial\chi}{\partial x}\right|_r^{(i,j)}=\frac{\chi(i,j)-\chi(i-1,j)}{2^{-r}}+O\left(2^{-r}\right),$$

just to mention a further example. The differences are normalized by the distance 2^{-r} between neighboring r-grid points, in x- or in y-direction. Larger neighborhoods could be used for defining more complex forward or

backward approaches, and further approaches may also be based on symmetric, or unbalanced neighborhoods of r-grid points. Finally, a finite difference scheme is characterized by selecting one approach for the x-, and an other one for the y-direction.

The *forward-forward FDS* transforms the given differential equation into

$$a \cdot \frac{\chi_r(i+1,j)-\chi_r(i,j)}{2^{-r}} + b \cdot \frac{\chi_r(i,j+1)-\chi_r(i,j)}{2^{-r}} + O\left(2^{-r}\right) = E\left(i2^{-r}, j2^{-r}\right),$$

and this equation may be simplified as

$$\tilde{\chi}_r(i,j+1) = \left(1+\tfrac{a}{b}\right) \cdot \tilde{\chi}_r(i,j) - \tfrac{a}{b} \cdot \tilde{\chi}_r(i+1,j) + \tfrac{2^{-r}}{b} \cdot E\left(i2^{-r}, j2^{-r}\right),$$

where $\tilde{\chi}_r(i,j)$ is used as an approximation for function $\chi_r(i,j)$. The *backward-forward FDS* leads to

$$\tilde{\chi}_r(i,j+1) = \left(1-\tfrac{a}{b}\right) \cdot \tilde{\chi}_r(i,j) + \tfrac{a}{b} \cdot \tilde{\chi}_r(i-1,j) + \tfrac{2^{-r}}{b} \cdot E\left(i2^{-r}, j2^{-r}\right),$$

the *forward-backward FDS* leads to

$$\tilde{\chi}_r(i+1,j) = \left(1-\tfrac{b}{a}\right) \cdot \tilde{\chi}_r(i,j) + \tfrac{b}{a} \cdot \tilde{\chi}_r(i,j-1) + \tfrac{2^{-r}}{a} \cdot E\left(i2^{-r}, j2^{-r}\right),$$

and the *backward-backward FDS* leads to

$$\tilde{\chi}_r(i,j) = \tfrac{1}{1+c} \cdot \tilde{\chi}_r(i,j-1) + \tfrac{c}{1+c} \cdot \tilde{\chi}_r(i-1,j) + \tfrac{2^{-r}}{b(1+c)} \cdot E\left(i2^{-r}, j2^{-r}\right),$$

where $c = \frac{a}{b} \neq -1$, and to

$$\tilde{\chi}_r(i-1,j) = \tilde{\chi}_r(i,j-1) + \tfrac{2^{-r}}{b} \cdot E\left(i2^{-r}, j2^{-r}\right)$$

otherwise for $c = -1$. These schemes were studied in [14, 15].

A finite difference scheme is *consistent* with an initial boundary value problem if the error of approximation in representing the original problem converges to zero as $2^{-r} \to 0$. The listed four schemes are consistent.

A finite difference scheme is *convergent* to the solution χ_r (if it exists) if the digitization error converges to zero as $2^{-r} \to 0$. A further notion of stability for linear difference schemes was defined by *Rjabenki* and *Filippov*, see [30]. A linear difference scheme is *RF stable* if the operators $\left\{R_r^{-1}\right\}_{r=0,1,2,\ldots}$ are *uniformly bounded* as $2^{-r} \to 0$.

General FDS Convergence Theorem [30, Theorem 5.1]**:** *A consistent and RF stable finite difference scheme is convergent to the solution of the given Cauchy problem if such a solution exists.*

For the convergence analysis of the given schemes let $c = \frac{a}{b}$ assuming that $b \neq 0$, and $d = \frac{b}{a}$ assuming that $a \neq 0$.

FDS RF Stability Theorem [14]**:** *The forward-forward FDS is RF stable iff* $-1 \leq c \leq 0$. *The backward-forward FDS is RF stable iff* $0 \leq c \leq 1$. *The forward-backward FDS is RF stable iff* $0 \leq d \leq 1$. *The backward-backward FDS is RF stable iff* $c \geq 0$ *or* $c = -1$.

Consequently (by the General FDS Convergence Theorem), in these positive cases the sequences of functions $\{\tilde{\chi}_r\}_{r=0,1,2,...}$ are convergent to the solution of the specified Cauchy problem. A few illustrations of shape recovery results were visualized in [14, 15] for synthetic input functions χ as the *volcano*

$$\chi_{volcano}(x,y) = 1 \Big/ \left(4\left(1 + \left(1 - x^2 - y^2\right)^2\right)\right)$$

and the mountain

$$\chi_{mountain}(x,y) = 1 \Big/ \left(2\left(1 + x^2 + y^2\right)^2\right)$$

where it was assumed that the shading values on these Jordan faces satisfy the linear image irradiance equation. A more complex function,

$$\chi_{hills}(x,y) = \frac{\sin(3x)^4 + \cos(2y)^4 + \sin(x+4y)^3 - \cos(xy)^5}{2} + 1,$$

is shown in Fig. 8.

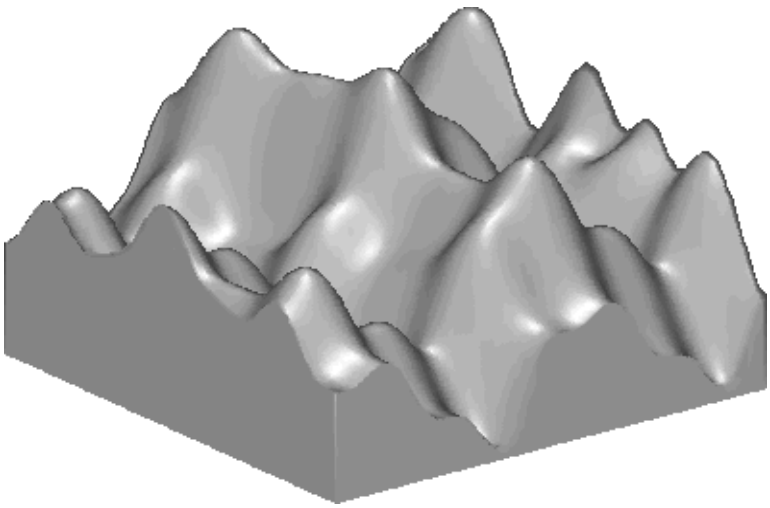

Figure 8 [2]**:** An example of a suggested function for testing different surface techniques.

Such functions may define a certain testbed for a more detailed comparison of the behavior of the different surface recovery techniques as the minimum Jordan surface calculation assuming a certain digitization method, the approximation of faces assuming a certain predefined explicit analytic shape, the recovery based on gradients generating gradients based on numeric differentiation, or the recovery based on solutions of differential equation systems assuming a specific object-surface reflectance model.

4 Conclusions

The discussed fundamental approaches "How to define a 3D surface?" as well as the given examples might be of interest for reconsidering some established approaches in digital geometry. For example, [29, property 1] define a *Jordan boundary* as a set which satisfies the Jordan surface theorem in 3D. Their boundary tracking algorithm for boundary faces of the cells of a given grid point set may be used for sound volume calculations, but not for sound surface area calculations. A *near-Jordanness property* (in short: every path from an element in the interior to an element of the exterior exits through the given set of polygons), see e.g. [6], was used in recent publications of *G. Herman, J. K. Udupa* et al. for discussing the partition of the digital space into an inside and an outside. A Jordan surface of a 6-connected cellular complex [8] satisfies the Jordan surface theorem because it is just a special case of a Jordan surface. It was proved, see [6], that the near-Jordanness property is useful for discussing algorithmic approaches for digital spaces.

The calculation of features of digital objects defined by voxel sets is certainly a topic in digital geometry. However the first example, the Jordan surface problem, should already point out that a model in continuous mathematics may help to propose a sound approach for feature calculation. The next examples did lead more and more away from the digital geometric case, ending with the study of a Cauchy problem at a numerical or analytical level of mathematics. However, in all these cases gridding techniques were applied, and the same soundness criterion was (successfully) tested. As a general hypothesis this leads to the opinion that different geometric approaches relevant to 3D object analysis will increasingly interact in the future. This is also expected at the computational level.

Recent interest in computational geometry develops also towards the study of efficacy (i.e. robustness or numerical stability) of geometric algorithms, see

[17]. The studied soundness constraints might be interpreted in this direction. The calculation of the minimum Jordan surface (Section 3.3.1) is related to convex hull problems in computational geometry [28], and should be of high interest in this area. The calculation of the least-square approximation plane (Section 3.3.2) belongs obviously to the class of geometric optimization problems, also studied in computational geometry. However, in [17] only the 2D case of polygonal curve approximation is cited in this class, and not this 3D computational problem. The gradient based recovery approach (Section 3.3.3) may also lead to interesting computational questions if combined with accuracy or approximation constraints.

The 3D shape description and recovery problem, based on digital input data, is a very multi-disciplinary problem. CAD systems apply a broad variety of digital surface representation techniques. Gridding techniques for differential equations, as briefly discussed in Section 3.3.4, are also studied in computational physics, see [35] - just to cite two fields different from 3D image analysis.

Acknowledgment

The co-authors of joint publications to topics sketched in this paper are Jovisa Zunic (Yugoslavia), Ivan Stojmenovic (Canada), Karsten Schlüns (New Zealand), and Ryszard Kozera (Australia). Fridrich Sloboda (Slovakia) made substantial contributions towards the subject sketched in Section 3.1 during his stay at Auckland University. I thank my colleague Richard Lobb for careful proofreading and commenting on the initial draft of this report.

5 References

1. I. W. Burr: *Applied Statistical Methods*. Academic Press, New York 1974.
2. S. L. Cheng: Estimation of volume and surface area from isosurface. Post-graduate project in computer science, 415.780 FC, University of Auckland, 1997.
3. F. Guliak: Volume and surface area measurement of viable chondrocytes in situ using geometric modelling of serial confocal sections. *J. of Microscopy* **173** (1994), pp. 245 - 256.
4. A. Jonas, N. Kiryati: Digital representation schemes for 3-d curves. CC Pub#114, July 1995, Dep. of Electrical Engineering, Technion - Israel Institute of Technology.

5. W. Heiden, T. Goetze, J. Brickmann: 'Marching cube' Algorithmen zur schnellen Generierung von Isoflächen auf der Basis dreidimensionaler Datenfelder. in: *Visualisierung von Volumendaten*, Springer, Berlin 1991, pp. 112 - 117.
6. G. T. Herman, E. Zhao: Jordan surfaces in simply connected digital spaces. http://www.unipissing.ca/topology/p/a/a/z/06.htm, *Topology Atlas* Preprint #54, 1996.
7. C. E. Kim: Three-dimensional digital line segments. *IEEE Trans. Pattern Anal. Mach. Intell.* **PAMI-5** (1983), pp. 231 - 234.
8. R. Klette: M-dimensional cellular spaces. CAR-TR-6, Univ. of Maryland, Center for Automation Research, College Park, August 1983.
9. R. Klette: The m-dimensional grid point space. *CVGIP* **30** (1985), pp. 1 - 12.
10. R. Klette, A. Koschan, K. Schlüns: *Computer Vision - Räumliche Information aus digitalen Bildern.* Braunschweig: Vieweg 1996.
11. R. Klette, I. Stojmenovic, J. Zunic: A parametrization of digital planes by least-squares fits and generalisations. *Graphical Models and Image Processing* **58** (1996), pp. 295 - 300.
12. R. Klette, K. Schlüns: Height data from gradient fields, Proc. *Machine Vision Applications, Architectures, and Systems Integration V*, SPIE 2908, Boston, Massachusetts, Nov. 18-19, 1996, 204-215.
13. J. Koplowitz: On the performance of chain codes for quantization of line drawings. *IEEE Trans. Pattern Anal. Mach. Intell.* **PAMI-3** (1981), pp. 180 - 185.
14. R. Kozera, R. Klette: Finite difference based algorithms for linear shape from shading. Machine Graphics & Vision (1997), to appear.
15. R. Kozera, R. Klette: Evaluation of finite difference algorithms for a linear shape from shading problem. Proceed. Advances of Visual Form Analysis, Capri, Italy, World Scientific (1997), pp. 330 - 339.
16. L. J. Latecki: Discrete Representation of spatial objects. in: *Advances in Digital and Computational Geometry* (R. Klette, A. Rosenfeld, F. Sloboda, eds.), Singapore, Springer - to appear.
17. D. T. Lee: Computational geometry. *ACM Computing Surveys* **28** (1996), pp. 27 - 31.
18. W. E. Lorensen, H. E. Cline: Marching cubes: a high resolution 3D surface construction algorithm. *Computer Graphics* **21** (1987), pp. 163 - 169.
19. H. v. Mangoldt, K. Knopp: *Einführung in die höhere Mathematik, III. Band, 12. Auflage.* Leipzig, S. Hirzel Verlag 1965.
20. R. A. Melter, A. Rosenfeld: New views of linearity and connectedness in digital geometry. *Pattern Recognition Lett.* **10** (1989), pp. 9 - 16.
21. R. A. Melter, I. Stojmenovic, J. Zunic: A new characterization of digital lines by least square fits. *Pattern Recognition Lett.* **14** (1993), pp. 83 - 88.

22. J. C. Roberts: An overview of rendering from volume data including surface and volume rendering. University of Kent at Canterbury, TR, December 1993.
23. A. Rosenfeld, A. C. Kak: *Digital Image Processing (2nd ed.)*. Academic Press, New York 1982.
24. A. Rosenfeld: Digital geometry - a bibliography. in: *Advances in Digital and Computational Geometry* (R. Klette, A. Rosenfeld, F. Sloboda, eds.), Singapore, Springer - to appear.
25. W. Scherer: Ein Satz über Gitter und Volumen. *Mathematische Annalen* **86** (1922), pp. 99 - 107.
26. W. Skarbek: Generalized Hilbert scan in image printing. in: Theoretical Foundations of Computer Vision (R. Klette, W. Kropatsch, eds.), Akademie Verlag, Berlin 1992, pp. 47 - 58.
27. F. Sloboda, B. Zat'ko: Piecewise linear approximation of planar Jordan curves and arcs: theory and applications. in: Computing Supplement 11 (W. Kropatsch, R. Klette, F. Solina, eds.), Springer, Wien 1996, pp. 183 - 200..
28. F. Sloboda: On approximation of Jordan surfaces: a topological approach. Internal Memo, CITR group, Tamaki, The University of Auckland, May 1997.
29. J. K. Udupa, V. G. Ajjanagadde: Boundary and object labelling in three-dimensional images. *CVGIP* **51** (1990), pp. 355 - 369.
30. P. J. Van der Houwen: Finite difference methods for solving partial differential equations. Mathematical Centre Tracts 20, Mathematisch Centrum Amsterdam 1968.
31. K. Voss: *Discrete Images, Objects, and Functions in Z^n*. Berlin, Springer 1993.
32. K. Voss: Discrete integral geometry and stochastic images. in: *Advances in Digital and Computational Geometry* (R. Klette, A. Rosenfeld, F. Sloboda, eds.), Singapore, Springer - to appear.
33. J. Wilhelms, A. V. Gelder: Topological considerations in isosurface generation. Baskin Center for Computer Engineering and Information Sciences, University of California, Santa Cruz, 94, UCSC-CRL-94-31.
34. G. Wyvill, C. McPheeters, B. Wyvill: Data structures for soft objects. *The Visual Computer* **2** (1986), pp. 227 - 234.
35. D. P. Young, R. G. Melvin, M. B. Bieterman: A locally refined rectangular grid finite element method: application to computational fluid dynamics and computational physics. *J. of Comp. Physics* **92** (1991), pp. 1 - 42.